

Comparisons of thick-target bremsstrahlung calculations by EGS4/PRESTA and ITS version 2.1

Bruce A. Faddegon and D.W.O. Rogers

Institute for National Measurement Standards, National Research Council of Canada, Ottawa, Canada K1A 0R6

Received 21 April 1992 and in revised form 3 November 1992

Two Monte Carlo codes, EGS4/PRESTA and ITS version 2.1, have been used to calculate spectral distributions of bremsstrahlung and annihilation quanta in 10–30 MV beams from thick targets of Be, Al, and Pb. Spectra are absolute (photons per incident electron) and calculated in 44 annular regions of 1° widths, covering all angles. It was found necessary to do ITS calculations using shortened sub-step sizes for electrons near the target surface to remove a 30–40% error in the angular distribution of bremsstrahlung at small angles that occurs when using default sub-step sizes. The EGS calculations were done using the enhancement which randomly samples the bremsstrahlung angle from an appropriate distribution and giving due consideration to K-shell X-rays. A survey is done of the remaining discrepancies in the spectral distributions of fluence, the total fluence and the mean energies of each spectrum. In general, EGS and ITS agree to $\pm 20\%$ for fluence and $\pm 5\%$ for mean energy. Results are compared to a set of high-precision measurements of absolute thick-target bremsstrahlung spectra used previously to show that EGS is reliable to $\pm 10\%$ for fluence and $\pm 2\%$ for mean energy. The measurements did not clearly identify a strong preference towards either EGS or ITS.

1. Introduction

The spectral distribution of bremsstrahlung from electrons incident on thick targets is of considerable interest in many aspects of radiation physics and is of fundamental interest in radiation therapy for the treatment of cancer. The photon spectrum originating in the target of a radiotherapy linear accelerator strongly influences the dose distribution in the patient and the response of dosimeters placed in the beam. Knowledge of the spectrum is a prerequisite for accelerator design (see, eg. ref. [1]), accurate treatment planning (see, eg. ref. [2]), and dosimetry (see, eg. ref. [3]).

The most accurate method for calculating thick-target bremsstrahlung is with Monte Carlo techniques [4]. The EGS system [5,6] and ETRAN [5,7] are standards for Monte Carlo calculations of radiation transport and have both been used for thick-target bremsstrahlung calculations (see, eg. refs. [1–18]). The Monte Carlo system used in this study is version 2.1 of ITS [5,8], a general purpose version of ETRAN which has undergone considerable development to make it a widely used tool for radiation transport studies. Previous comparisons of ETRAN and EGS3 found in the EGS3 manual [9] have shown significant differences in the total bremsstrahlung fluence of between 15–30% in the forward direction and as high as 50% at back angles for 20–30 MV beams from thick targets of high atomic number (see also fig. 13.11 of ref. [5]).

We have recently used a large NaI detector to measure a comprehensive set of thick-target bremsstrahlung spectra [4,17,18]. Beam energies varied from 10–30 MV, the range of interest in radiation therapy, as well as the region of greatest uncertainty in theoretically determined bremsstrahlung cross sections [11,12]. The measured spectra were absolute (photons per incident electron), of high resolution (limited by the detector resolution, 5% FWHM at 20 MeV), and accurate to $\pm 5\%$ in the total fluence. Spectra were measured for 15 MV beams from Be, Al, and Pb targets at eight angles ranging from 0° to 90° relative to the beam axis, and for 10–30 MV beams from Al and Pb targets at 0° . Comparisons were made with the results of detailed EGS4 simulations of the experiment. The simulations included the small amount of material upstream of the target which was necessary for measurement of the beam current and made a considerable contribution to the bremsstrahlung intensity in a small angular range about the forward direction. The measurements agreed with EGS4 to $\pm 10\%$ for the fluence per incident electron and to $\pm 2\%$ for the mean energies. This level of agreement is consistent with the estimated 10% accuracy of bremsstrahlung cross sections used in the simulations, although this does not rule out possible problems with the particle transport.

With the availability of quality measured spectra, the demonstrated success of EGS in simulating these

spectra, and knowledge of the discrepancies found between earlier versions of the two codes, it is of considerable interest to compare ITS version 2.1 to both EGS4 and measurement in the same energy range as our experimental studies. This is done in the current study where we compare calculations of bremsstrahlung spectra in a simple geometry, namely, thick cylindrical targets in a vacuum. The calculated spectra have better energy and angular resolution and cover a more comprehensive set of angles, targets, and beam energies than those from previous studies. The ITS spectra are compared to the measured spectra indirectly by taking ratios of ITS results to EGS results for a target in a vacuum and comparing these to ratios of measurements and EGS results for the more complicated experimental geometry. This reduces the sensitivity of the comparison of the ITS and measured spectra to the different target radii used in the two studies and to the material upstream of the target in the experiment.

One difference in the approaches used for transporting electrons in ITS and EGS is of considerable importance to bremsstrahlung calculations. In ITS, each electron step is divided into a number of sub-steps. A bremsstrahlung event is randomly sampled at a position along a sub-step and the electron direction at the point of bremsstrahlung production is taken to be that at either the beginning or the end of the sub-step, whichever is closer to the point of production. Therefore, bremsstrahlung photons are occasionally generated relative to the electron direction at the surface of the target, before the electron has had an opportunity to scatter. Due to the highly forward-directed nature of bremsstrahlung from relativistic electrons and the strong effects of electron multiple scattering, a normally incident electron beam can yield an unrealistically narrow beam of photons unless the mean scattering angle of the electron in the first sub-step is much less than the mean angle of bremsstrahlung emission, which is the ratio of the rest mass of the electron to its energy, mc^2/E . In order to achieve a realistic angular distribution with ITS in this study, the sub-step size was reduced to about 1/5 of the default size.

2. Materials and method

2.1. Simulated beams

Monoenergetic electron beams of 10, 15, and 30 MeV with 0.05 cm radii were normally incident on the central axis of Be, Al, and Pb targets. The target dimensions were chosen to prevent primary electrons from escaping the sides or back (downstream surface). Target thicknesses (table 1) correspond to those used in our previous experimental studies. All targets had the same radius of 9.63 cm for ease in defining the

Table 1

Simulation parameters. Target densities were 1.850 g/cm² (Be), 2.700 g/cm² (Al), and 11.34 g/cm² (Pb). Target radii were 17.82 g/cm² (Be), 26.0 g/cm² (Al), and 109.2 g/cm² (Pb). The number of electron histories followed in the ITS simulations are for those simulations done using shortened sub-steps (see text). The 'Brem Factor' is the number of photons generated per bremsstrahlung event for EGS and the cross section scaling factor for ITS

Energy [MeV]	Target	Thickness [cm]	Histories		Brem Factor	
			EGS	ITS	EGS	ITS
			($\times 10^6$)	($\times 10^6$)		
10	Be	3.80	7.4	0.63	30	32
	Al	2.40	3.2	0.44	30	30
	Pb	0.60	0.5	0.2	30	28
15	Be	6.30	2.4	0.90	30	31
	Al	3.60	0.90	0.40	30	12
	Pb	0.805	0.60	0.25	20	3
30	Be	10.00	0.75	0.35	30	30
	Al	6.00	0.60	0.20	30	30
	Pb	1.200	0.67	0.20	5	5

scoring regions in the simulations. The number of electron histories followed in each simulation (table 1) was chosen to give simulation times of approximately 100 h. The ITS simulations were run on a μ VAX-3600 and the EGS simulations on a Sun Sparc-station 1, which was twice as fast. This enabled more histories to be run for the EGS simulations and resulted in a higher precision.

2.2. Fluence scoring

Spectral distributions of the photon fluence were accumulated in the scoring regions. In the EGS simulations, electron and positron spectra were also accumulated, as well as the mean energies of each particle type. In both ITS and EGS simulations, spectra were accumulated in 44 annular regions of 1° widths, concentrated along the beam axis. The 0° and 180° scoring regions are cones with a half-angle of 0.5°. The scoring regions were symmetric about the horizontal plane through the target surface to simplify the geometry. Scoring in the annular regions from 0–89° and 91–180° was done along two planar regions 100 cm downstream and upstream of the front of the target, respectively, and from 89–91° along a cylindrical surface 5730 cm from the central axis of the target.

The quantity scored was the total path-length of each particle type in each energy bin through the scoring volume (annular regions bounded by two coplanar surfaces 0.1 cm apart) per unit volume. This is equivalent to the differential fluence. The fluence was distributed into 70 logarithmically-spaced energy bins

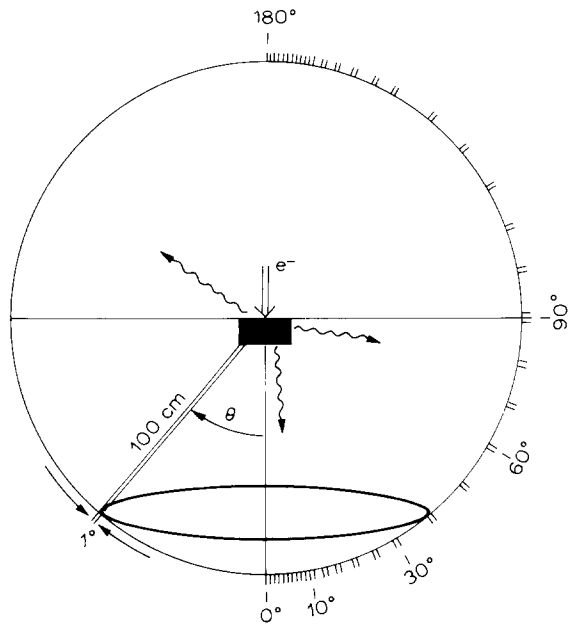


Fig 1. The simulation geometry and fluence calculation regions. Narrow beams of monoenergetic electron were normally incident on the central axis of thick targets placed in a vacuum. The spectral distribution of fluence was calculated in the 44 annular regions of 1° widths shown here. Fluence was calculated 100 cm from the center of the front surface of the target.

from the incident electron energy down to 1 keV. The wider energy bins at higher energies compensated for the reduced fluence and helped to maintain reasonable precision. The inverse square law was applied to determine the spectral distribution of fluence at 100 cm, denoted by $\Phi_E(\theta)$, which was calculated in the 44 annular regions shown in fig. 1.

The following spectral-integrated quantities were calculated from $\Phi_E(\theta)$:

1) The fluence,

$$\Phi(\theta) = \int_{E_0}^{E_c} \Phi_E(\theta) dE \quad [\text{cm}^{-2}], \quad (1)$$

where E_c is the incident electron energy.

2) The mean energy,

$$\bar{E}(\theta) = \frac{1}{\Phi(\theta)} \int_{E_0}^{E_c} \Phi_E(\theta) E dE \quad [\text{MeV}]. \quad (2)$$

3) The energy fluence,

$$\Psi(\theta) = \int_{E_0}^{E_c} \Phi_E(\theta) E dE = \Phi(\theta) \bar{E}(\theta) \quad [\text{MeV cm}^{-2}]. \quad (3)$$

These quantities were calculated as summations over the energy bins. The mean energies calculated in this

manner were the same within the precision of the calculations as those scored directly, as done in the EGS simulations.

2.3. EGS4 simulations

The EGS4 simulations were done with the user-code FLURZ using the PRESTA boundary-crossing algorithm [19], as in our previous studies. Electrons were followed down to 1.0 MeV kinetic energy and photons down to 1 keV. The angle of the bremsstrahlung photon relative to the incoming electron was sampled from the Schiff distribution (eq. 2BS of ref. [20]). Bielajew et al. [21] have recently made this option available in EGS4, which is essential to obtain the correct bremsstrahlung angular distribution [4,21]. To improve the efficiency of the calculations, up to 30 photon histories were initiated for each bremsstrahlung event (table 1). This number was reduced for the high atomic number target at higher energies simply to keep the number of particles being followed at any one time below an arbitrary particle-stack limit of 125. These photons and their ancestors were weighted appropriately to give the correct fluence per incident electron.

Both the collisional and radiative stopping powers used with EGS4 in this study are based on those of ICRU report 37 [11,22,23]. In the case of radiative stopping powers, this was done by scaling the differential cross sections so that the radiative stopping powers, which are determined from the integral of the bremsstrahlung cross sections over solid angle and photon energy, agree with those of ICRU 37. However, the differential cross sections still differ from those of Seltzer and Berger [12], which were used in ICRU 37 for calculating radiative stopping powers.

The step size of charged particles chosen by the PRESTA algorithm can be reduced by lowering the value of the step-size parameter, BLCMIN. Shortened initial step-sizes were used for one full set of simulations, as in our previous studies [4,18], and the default values were used for a second full set of simulations, both with the level of precision of the results shown in this study. The results agreed within the precision of the calculations, thus the default choice is acceptable.

2.4. ITS simulations

The ITS simulations were done using version 2.1 of December 9, 1987, using the CYLTRAN code. The same electron and photon energy cut-offs were used as in the EGS4 simulations. The bremsstrahlung cross section was scaled to give a comparable number of photons per bremsstrahlung event as the EGS4 simulations (table 1). Products of photon interactions were discarded by Russian Roulette so that only the natural

numbers of electrons and positrons were followed. This Russian Roulette was not done in the EGS simulations.

Simulations were repeated for all targets and energies with two different sub-step sizes: the default size and shortened sub-steps. For Be and Al the sub-step sizes were 20% of the default sizes and for Pb, 15% of the default size. The short sub-step runs (table 1) took about twice as long as runs using the default sub-step sizes when large bremsstrahlung scaling factors were used, but nearly 5 times as long for the 15 MV simulation for the Pb target, which uses a small scaling factor. Since the anomaly is a surface effect, computing time was saved in the simulations of the Pb targets by dividing the target into two slabs, a thin initial layer in which shortened sub-steps were used followed by the remainder of the target in which default sub-step sizes were used. The size of the initial layer was sufficient for the electron beam to achieve a mean scattering angle equal to the mean bremsstrahlung angle. Mass scattering powers [24] were used to determine this thickness for the Pb target: 0.09 g/cm² at 10 MeV, 0.13 g/cm² at 15 MeV, and 0.23 g/cm² at 30 MeV. A comparison was made for the 15 MV beam where this approach gave results which agreed with those obtained using shortened sub-steps throughout the slab and was nearly as efficient as the simulation using the default sub-step size, taking only 5% longer to run the same number of histories.

3. Results and discussion

3.1. Energy fluence

Angular distributions of the energy carried by the photon component of the simulated beams are shown in fig. 2. The energy fluence of bremsstrahlung at small angles is roughly independent of atomic number of the target due to a trade-off between increased bremsstrahlung cross section with atomic number and increased angular scattering of electrons with atomic number. The latter spreads the bremsstrahlung beam out more. The valleys at 90° are due to target self-absorption. The Pb targets in particular transmit little beam through the sides. There is much less angular variation in the energy fluence at back angles than at forward angles since the energy fluence at back angles is largely determined by bremsstrahlung from widely scattered electrons and from target scatter, both of which have wide angular distributions. Discrepancies between ITS and EGS are apparent for all of the targets at small angles, and for the Pb target at back angles. These are seen more clearly by looking at ratios of the fluence as shown later.

The energy fluence of annihilation radiation (511 keV) shown in fig. 2 was calculated from the photon

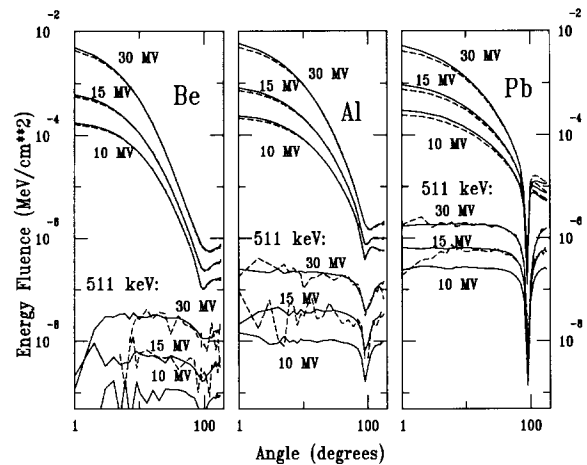


Fig. 2. Angular distributions of photon energy fluence calculated by EGS4 (solid lines) and version 2.1 of ITS (dashed lines) for 10, 15, and 30 MV bremsstrahlung beams from Be, Al, and Pb targets. The ITS simulations were done with shortened sub-steps. The higher precision obtained for the EGS results is due to the larger number of histories run for each simulation and should not be construed as a difference in the calculational efficiency of the two codes. The upper sets of curves include all photons above 1 keV. The lower sets of curves show the calculated energy fluence of annihilation radiation determined from a 2 keV energy bin centered on 511 keV, with background subtraction. The precision of the ITS results is sufficiently low at small angles that the 511 keV peak is swamped by the bremsstrahlung fluence. Background subtraction results in negative fluence at some of these angles, for the low atomic number targets in particular, and in these cases results at small angles are left off of the plots. For clarity, the ITS results for annihilation radiation from the 10 MV beams are not shown.

spectra as the fluence per unit energy in a 2 keV bin from 510 to 512 keV, less the average fluence per unit energy in the adjacent bins, multiplied by 1022 keV², the product of the bin width and the energy of the radiation. The annihilation radiation is much more isotropic than the bremsstrahlung and carries very little of the beam energy. The ITS results agree with those of EGS, but are of much poorer precision since positrons were Russian-Rouletted in the ITS simulations, but not in the EGS simulations.

3.2. Total fluence

3.2.1. Forward angles

The ratio of fluence from ITS to that of EGS is shown for the 15 MV beams at forward angles (0–90°) in fig. 3 and at 0° as a function of beam energy in fig. 4. The results shown are for targets, energies and angular ranges for which precision measurements were available for comparison. The comparisons of the calcu-

lated fluence shown in these figures are representative of all of the beams.

Shortening the sub-step size used in the ITS simulations results in a more realistic angular distribution at

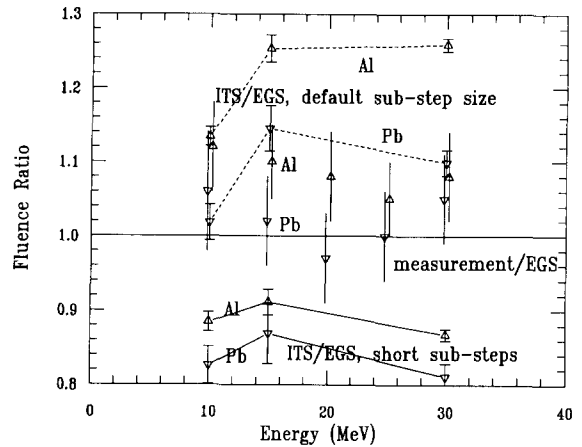
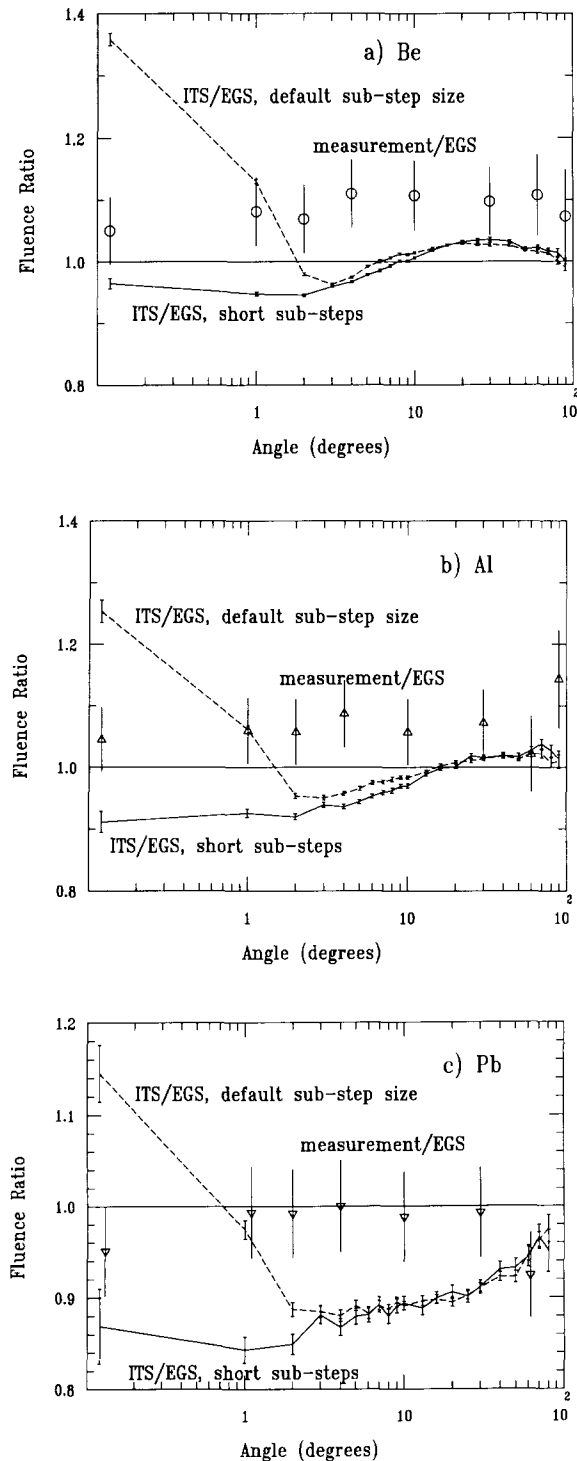


Fig. 4. Fluence ratios along the beam axis in the angular bin from $0-0.5^\circ$ for 10–30 MV beams from Al (Δ) and Pb (∇) targets. ITS results (lines) and measurements (points) are shown relative to EGS results. ITS simulations were done using both the default sub-step size (dashed lines) and shortened sub-steps (solid lines). Photons with energies down to 1 keV are included in the fluence. For the experimental comparisons, EGS simulations were done to conform closely to the experimental geometry, and photons below 220 keV were excluded from the fluence. The measurements show no clear preference for either EGS or ITS.

small angles. The results in fig. 3c for a 15 MV beam from a Pb target imply a 30% error in the beam flatness over a 10 cm by 10 cm field at 100 cm from the target, when the default sub-step size is used. This field is typical in radiation therapy. The effect is larger for targets of lower atomic number (35% for Al and 40% for Be) and is similar for beam energies ranging from 10 to 30 MV. Shortening the sub-step size has no discernible effect on the fluence at angles larger than the mean bremsstrahlung angle. In ITS, the default length of the electron sub-step for 30 MeV electrons is 0.7 g/cm^2 for Be, 0.2 g/cm^2 for Al, and 0.04 g/cm^2 for Pb. The first half of the sub-step is then 8 to 10

Fig. 3. Fluence ratios at forward angles for 15 MV beams from targets of (a) Be, (b) Al, and (c) Pb. ITS results (lines) and measurements (points) are shown relative to EGS results. ITS simulations were done using both the default sub-step size (dashed line) and shortened sub-steps (solid line). For the calculational comparisons (ITS/EGS), photons with energies down to 1 keV are included in the fluence. For the experimental comparisons (measurement/EGS), EGS simulations were done to conform closely to the experimental geometry, and photons below 145 keV were excluded from the fluence. The measurements show no clear preference for either EGS or ITS. The calculated results at right angles for the Pb target are of poor precision and are not shown (see text). Some points are offset for clarity.

times smaller than the thicknesses at which the mean scattering angle of 30 MeV electrons equals the mean bremsstrahlung angle, as calculated from the mass scattering power. Even so, use of the default sub-step size results in an unrealistic angular distribution. With the sub-step size reduced by a factor of 5 or more the error is essentially eliminated since very few photons are generated at the surface, the angular distribution of these photons is completely dominated by the bremsstrahlung cross section, and electron scattering contributes to the angular distribution of the photons generated beyond the first half sub-step.

In EGS, bremsstrahlung interrupts the step and is emitted after electron multiple scattering has occurred, so the step size does not have the same effect as in ITS. However, a related effect does result in an error in the angular distribution of bremsstrahlung at small angles which is of similar magnitude to the sub-step size artifact in ITS. This occurs when the bremsstrahlung photon is emitted at a fixed angle (mc^2/E) instead of an angle randomly sampled from a more realistic distribution [4,21], as done in this study.

When shortened sub-steps are used with ITS, the largest discrepancies in the calculated fluence between ITS and EGS at forward angles occur at 0° in the 30 MV beams: $(13 \pm 1)\%$ for both Be and Al and $(19 \pm 2)\%$ for Pb. This is well outside the statistical precision of the calculations. Uncertainties quoted in this paper are one standard deviation.

Comparisons between measurements and EGS that we have previously reported [4,18] are also shown in figs. 3 and 4. The EGS simulations done for these comparisons accounted for the complexities of the experimental geometry. The 90° result for Pb, which is left off of fig. 3c, was not considered relevant to this study due to the vastly different target radius used in the earlier studies. The measurements were limited to energies above 145 keV for the angular distribution at 15 MV and 220 keV for the 10–30 MV measurements at 0° . Photons down to 1 keV were included in the calculational comparisons of the present study in order to get the highest precision available from the calculations. This has no impact on the comparison to the measurements since excluding photons below 220 keV in the spectral integrations did not significantly effect the ITS to EGS fluence ratios for the forward angles.

The measurements compare favourably with the EGS results, showing agreement to $\pm 10\%$. The ITS results shown in the same figures, normalized to the EGS results, are further away from the measurements at small angles, with discrepancies larger than $\pm 20\%$ at 0° (fig. 4). This suggests a preference for EGS at these angles. However, caution must be exercised when comparing the measurements directly to the ITS results due to the more complex geometry used in the experiments. In addition, the experimental uncertainty

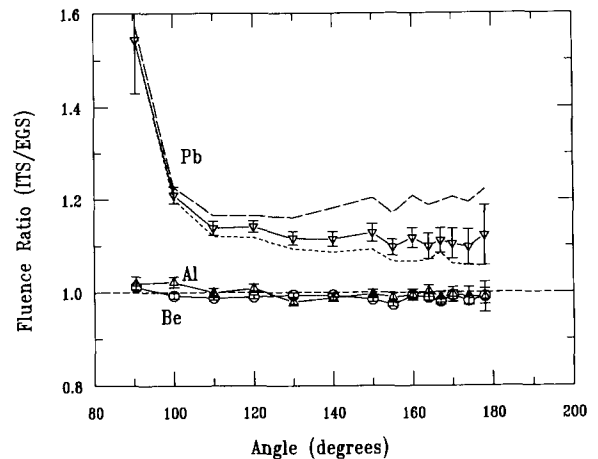


Fig. 5 Fluence ratios calculated by ITS and EGS at back angles for 15 MV beams from Be, Al, and Pb targets. The ITS results used here are from the simulations done using shortened sub-steps. When the default sub-step size was used the same results were obtained, within the precision of the calculations. The long-dashed line for Pb shows a comparison of ITS with fluorescent X-rays to an EGS simulation done with no fluorescent X-rays generated. The difference between the long-dashed line and the solid line is the relative contribution of K-shell X-rays from the photo-electric effect to the fluence at each angle. Photons down to 1 keV are included in the fluence determinations except for the short-dashed line for Pb, which excludes photons below 100 keV. The difference between the solid line and the short-dashed line is approximately the relative contribution of K-shell X-rays from electron-impact ionization to the fluence at each angle. Electron-impact ionization was not simulated by EGS.

of $\pm 5\%$ makes it difficult to discriminate between EGS and ITS on the basis of these comparisons.

3.2.2. Back angles

Fluence ratios calculated at back-angles for the 15 MV beams are shown in fig. 5. Similar results were obtained for the 10 and 30 MV beams. Consider the results for the Be and Al targets first. The EGS and ITS results for these targets agree within two standard deviations of the precision of the calculations (typical uncertainties are shown in fig. 5), except for the 30 MV beam from Be (not shown). In this case the fluence calculated at angles from $100\text{--}180^\circ$ by ITS is $(6 \pm 1)\%$ lower than that calculated by EGS.

The largest discrepancies are for the Pb targets. Excluding K-shell X-rays from the comparisons (short-dashed curve in fig. 5), ITS calculates a 10–15% higher fluence than EGS from $115\text{--}180^\circ$, the lower value corresponding to the 10 MV spectra. Including the 5–20% fluence difference for the forward angles, which is in the opposite direction, ITS calculates a 25% greater change in the fluence between forward and

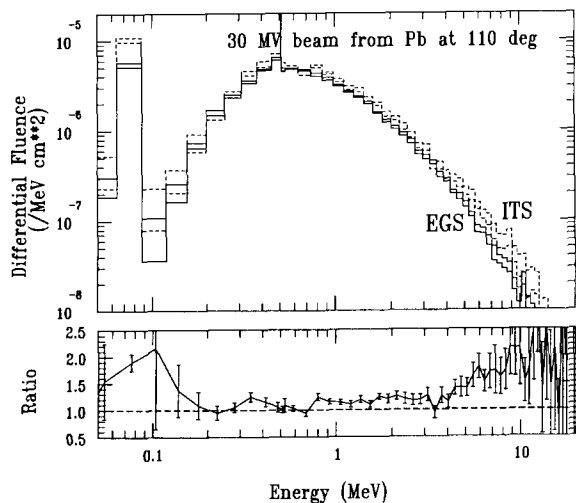


Fig. 6. Bremsstrahlung spectral distribution at 110° for 30 MeV electrons on Pb. The differential fluence at 100 cm is shown in the upper plot: solid histograms – EGS, dashed histograms – ITS. The lower and upper curves of each spectrum are bounds of the 68% confidence intervals (calculational precision). The annihilation radiation peaks are off the scale of the plot. K-shell X-rays are accumulated in the 64–88 keV energy bin. Differential fluence ratios are shown in the lower plot. The total fluence calculated by ITS for this beam at this angle was $(15 \pm 2)\%$ greater than the EGS result and the mean energy was $(13 \pm 2)\%$ greater than the EGS result, restricted to energies above 100 keV. The discrepancies in these quantities are among the largest found in this study.

back angles than calculated by EGS. This difference is unrelated to the use of shortened sub-steps in ITS, which has little effect on the fluence ratios at back angles. These discrepancies could potentially be resolved by experiment.

Characteristic X-rays from high atomic number targets play a significant role at back angles, as seen in fig. 5. A direct analysis of the ITS spectra, such as the spectrum shown in fig. 6, shows that K-shell X-rays from Pb contribute up to 10% of the fluence at back angles for 10–30 MV beams, and that the fluence of these X-rays increases roughly linearly with angle between 90° and 180° and roughly with the square of the beam energy between 10 MV and 30 MV. The fluence of K-shell X-rays at 180° , as calculated by ITS, was $6.5 \times 10^{-7} \text{ cm}^{-2}$ at 10 MV, $1.2 \times 10^{-6} \text{ cm}^{-2}$ at 15 MV, and $6.5 \times 10^{-7} \text{ cm}^{-2}$ at 30 MV. These X-rays are from both the photo-electric effect and electron impact ionization. The latter is simulated by ITS, but not by EGS. ITS produces approximately 50% more fluorescent X-rays than EGS at back angles (see e.g., fig. 6), and these are due to electron impact ionization, assuming both codes produce the same number of X-rays by the photo-electric effect. This is a reasonable assumption since the codes calculate the same fluence of

fluorescent X-rays at forward angles where the electron fluence is low and the contribution of X-rays from electron impact ionization is negligible.

3.2.3. Right angles

The beam energy fluence reaches a minimum at right angles, as seen in fig. 2, due to self-absorption in the targets. In the Pb spectra there is an abrupt change in fluence between 89.5° and 90.5° , a factor of 4 increase in the 10 MV beam as calculated by ITS. This is due to the high absorption of photons produced in or scattered from the surface of the Pb target which are directed towards the $89\text{--}90^\circ$ angular bin compared to those directed towards the $90\text{--}91^\circ$ angular bin, since the latter need not traverse the full width of the target. The fluence calculated at 89.5° is in generally good agreement, however, EGS consistently calculates a lower fluence than ITS at 90.5° ranging from $(25 \pm 10)\%$ lower for the 30 MV beam to $(50 \pm 6)\%$ lower for the 10 MV beam. We attribute these discrepancies to problems with numerical precision in the geometry routines for this unphysical geometry.

3.3. Mean energies

The mean energy is an indicator of the level of agreement between spectral shapes calculated by the two codes. Spectral shapes depend not only on the differential bremsstrahlung cross sections but also on the relative contribution of bremsstrahlung from electrons of different energies and trajectories and of scattered photons, which are affected by the details of the simulated particle transport.

Representative plots of the mean spectral energies are shown in fig. 7. Photons down to 1 keV were included in the ITS/EGS comparison for Be to obtain the highest precision for the mean energy ratios at back angles. This had limited impact on the comparison to measurements since excluding photons below 145 keV, the lowest energy in the spectral measurements, made little difference in the ratios of mean energies from the calculated spectra at forward angles, where the precision on the calculation remained high. For Pb, photons below 145 keV were excluded from the mean energy calculations to facilitate a more direct comparison to the measurements.

Results of ITS (using shortened sub-steps) and EGS for all targets and beam energies generally agree to within $\pm 5\%$ or 3 standard deviations statistical uncertainty, with the exception of the 30 MV beam from Pb at back angles. The maximum discrepancies occur at back angles. In this region, ITS results for Be ranged from $(5 \pm 2)\%$ lower than EGS results for the 10 MV beam to $(3 \pm 2)\%$ higher for the 30 MV beam, ITS results for Al from $(6 \pm 2)\%$ lower than EGS results

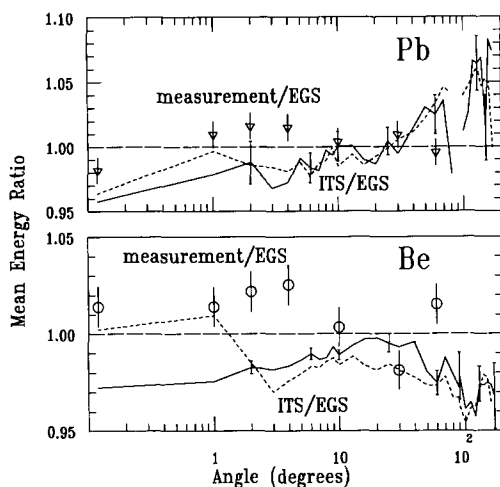


Fig. 7. Ratios of mean energies of 15 MV bremsstrahlung beams from Be and Pb targets. EGS is compared to ITS using the default sub-step size (short-dashed lines) and shortened sub-steps (solid lines). Measurements (points) are also compared to EGS using the experimental geometry in the simulations. For Pb, photons below 145 keV are excluded from the mean energy calculation, consistent with the measurements. For Be, photons down to 1 keV are included in the ITS/EGS comparisons for improved precision. The measurements show no clear preference for either EGS or ITS. The calculated results at right angles for Pb are of poor statistical precision and are left off of the plot.

for the 30 MV beam to $(3 \pm 2\%)$ higher for the 15 MV beam, and ITS results for Pb were all higher than EGS results with the largest discrepancies of $(10 \pm 3\%)$ for the 30 MV beam from $100\text{--}140^\circ$. Results at angles over 170° for all targets and at right angles for Pb have been ignored in these general comparisons due to poor calculational precision. For the Pb targets, photons below the K-edge were excluded from the calculated ratios to remove K-shell X-rays due to electron impact ionization from the comparison, since these are considered in ITS, but not in EGS.

The lower mean energies calculated by ITS at small angles are a reflection of the fewer photons at high energies relative to EGS results as discussed later. This may be related to the step-size artifact in ITS since in some cases the sub-step size had a significant effect on the spectral shapes at small forward angles, as seen by the effect on the mean energies at 0° and 1° for the 15 MV beam from Be shown in fig. 7.

The nature of the discrepancy for the 30 MV beam from the Pb target is seen more clearly by comparing the calculated bremsstrahlung spectra as done in fig. 6. For this spectrum, excluding K-shell X-rays, ITS calculates 15% more fluence and 13% greater mean energy than EGS. The figure shows this is due to an increase

in the absolute number of photons generated by ITS above 1 MeV, relative to those generated by EGS.

Measurements are also compared to EGS results in fig. 7. The EGS results generally agree with the experiment within $\pm 2\%$. The ITS short sub-step results are further away from the measurements than this, although the precision on the comparison is not very high. These results indicate a preference for EGS over ITS. However, it is difficult to draw clear conclusions from these comparisons for the same reasons as discussed earlier.

3.4. Spectra

Spectra from the 15 MV Al simulations are shown in fig. 8. The general trends are duplicated in all of the beams:

- 1) There is generally good agreement between the spectral shapes calculated by EGS and ITS.
- 2) The 0° spectra are noisy due to the small solid angle subtended by the scoring region, especially the ITS spectra which are calculated from fewer histories.
- 3) Self-absorption in the targets results in a turnover point in each spectrum which occurs at 20 keV in Be, 80 keV in Al, and 500 keV in Pb, independent of beam energy.

Comparisons were done of the full set of spectral distributions calculated by ITS and EGS for this study. These results comprise a large number of points (70 energy bins, 44 angles, three beam energies, three targets). Comparison of the spectral distributions was

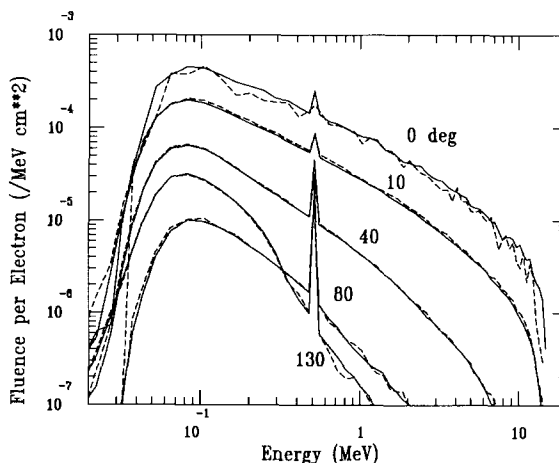


Fig. 8. Spectral distributions of bremsstrahlung from a 2.40 cm thick Al target bombarded with 15 MeV electrons as calculated with EGS (solid lines) and ITS (dashed lines) at selected angles. The positron annihilation radiation (511 keV) is distributed in a 2 keV energy bin. The higher precision obtained for the EGS results is due to the larger number of histories run for each simulation and should not be construed as a difference in the calculational efficiency of the two codes.

aided by a compilation of plots of selected spectra and their corresponding differential fluence ratios [25]. The study has revealed that the major discrepancies between the codes can be seen on selected plots of differential fluence, total fluence, and mean energies, which have already been presented.

The following analysis ignores ratios with statistical uncertainties greater than 10% or isolated ratios up to a few standard deviations from unity that are not part of a trend. Consider the angular range 0–10° first. The minimum differential fluence ratios occurred at these angles and typical worst case ratios for individual photon energies were between 0.65–0.7 for each beam. This is reflected in discrepancies in the total fluence, as seen in fig. 3. There are also significant discrepancies in the spectral shapes calculated at these angles. For each beam there was a gradual change in the differential fluence ratios between the turnover point and the upper end of each spectrum, with ITS producing relatively fewer high-energy photons than EGS, which results in a lower mean energy, as seen in fig. 7. The largest variations of this type occurred in the 10 MV beams: an average 10% variation across each spectrum for Be, Al and Pb. There was also a more sudden 10–15% change in the differential fluence ratios in the 10 and 15 MV Be spectra at small angles which is in the same direction as the gradual variation and occurs between 7 and 9 MeV in the 10 MV spectra and between 11 and 13 MeV in the 15 MV spectra. There is an indication of similar anomalies in the 10 and 15 MV Al spectra, but these are limited to only 1 or 2 points and could be simply statistical fluctuations. This anomaly is not present in the Pb spectra.

The maximum differential fluence ratios of 2.0 occurred at back angles for the Pb targets in the energy bin which contained the 88 keV K-shell X-rays, as seen in fig. 6. If characteristic X-rays are excluded from the comparisons, the differential fluence ratios at back angles for the beams from the Pb targets vary from 0.9 to 1.5. This is reflected in significant discrepancies in both the fluence and the mean spectral energies. For example, ITS calculates a higher differential fluence of high-energy photons than EGS at 110° in the 30 MV beam from Pb, as shown in fig. 6, and this results in a significantly higher fluence and mean energy at this angle.

In most cases the ratios of differential fluence did not vary by much more than $\pm 10\%$ within any beam at any given angle in regions of 10% or better precision. Larger variations did occur in regions of low fluence at either end of each spectrum where the precision approached 10%. For example, 30–40% variations in the differential fluence ratios occurred in the 30 MV beam from Pb at small angles, but these are generally statistical fluctuations at the upper end of the spectrum where the precision is low.

4. Summary and conclusions

A comprehensive set of high-resolution 10–30 MV bremsstrahlung spectra from thick targets have been calculated using two Monte Carlo systems: EGS4 and version 2.1 of ITS. Comparisons were made of the differential fluence at each angle within each beam and of the angular distributions of energy fluence, fluence, and mean energy. The bremsstrahlung spectral distributions were calculated with sufficient precision to discern variations in the differential fluence within each spectrum of 10% or more. The EGS results are of higher precision than the ITS results simply because a faster computer and more histories (table 1) were used to calculate the EGS results. A comparison of the calculational efficiencies of these two codes was not done in this study. Rather the study focusses on the accuracy of the calculations by comparing high-precision results of narrow angular resolution obtained from the two codes and from measurements.

Significant differences were found in the spectral shapes at small angles which were more pronounced for the 10 MV beams, and at back angles for the beams from Pb. The total fluence of the spectra calculated for each target, beam energy, and angle generally agreed to within $\pm 20\%$, and the mean energies of these spectra to within $\pm 5\%$ or 3 standard deviations. There were 25% differences in the fluence ratios calculated by the two codes between forward and back angles in the 10–30 MV beams from Pb, which could potentially be resolved with measurements at back angles.

To obtain this level of agreement the sub-step size used by ITS must be reduced substantially from the default value for beams with angular spreads less than mc^2/E . This is important for simulations of electron beams normally-incident on any target for the calculation of fluence for typical radiotherapy fields. In addition, the EGS simulations must employ bremsstrahlung angular sampling and include K-shell X-rays, although the latter is only important for high-Z targets at back angles. It is also advisable to use the improved set of bremsstrahlung cross sections in EGS simulations since in certain instances this can effect the calculated fluence by more than 10% (see ref. [4]).

With these changes, better agreement is obtained between the ITS and EGS spectral distributions than reported in the EGS3 manual [9]. The fluence at forward angles out to 5° for the 30 MV beam from Pb is 15% lower when calculated with ITS than with EGS4, showing significantly better agreement than the previously calculated difference of 30% for the 30 MV beam from W, with ETRAN lower than EGS3. At 15 MV, ITS calculates 15% fewer photons than EGS4 for the Pb beam out to 5°. This is comparable to the difference between the ETRAN and EGS3 calculations previously reported for a 20.9 MV beam from a

composite target of W and Au. The fluence at back angles for the 30 MV beam from Pb is 15% higher when calculated with ITS than with EGS4, a large improvement over the 50% differences reported between the ETRAN and EGS3 results for a 30 MV beam from W. The overall improvement in the level of agreement between the two codes is attributed to the approaches used to simulate the beams in this study as well as differences between the version of the codes used in this study and those used in the earlier studies.

It would be interesting to compare the new version of ITS [26] to the EGS4 results reported in this study since they use similar bremsstrahlung cross sections, that is, the radiative stopping powers are both consistent with ICRU 37 [11], although the shapes of the differential cross sections used by the two codes still differ.

Comparison to precision measurements have previously shown EGS4 can simulate 10–30 MV bremsstrahlung beams with an accuracy of $\pm 10\%$ in the fluence and $\pm 2\%$ in the mean energies of the beams at forward angles. The agreement with ITS is generally not quite as good. This indicates a slight preference for spectra calculated using EGS4, which should not be taken too seriously due to the experimental uncertainties of $\pm 5\%$ and the complexity of the experimental geometry, which was not fully simulated in this study.

Acknowledgements

We would like to thank Dr. Carl Ross for his valued support in this project and Dr. Alex Bielejew for adapting EGS4 to UNIX systems. This work was supported in part by NIH grant No. R01 CA52692-02.

References

- [1] R.C. McCall, R.D. McIntyre and W.G. Turnbull, *Med. Phys.* 5 (1978) 518.
- [2] R. Mohan, C. Chui and L. Lidofsky, *Med. Phys.* 12 (1985) 592.
- [3] J.R. Cunningham and R.J. Schulz, *Med. Phys.* 11 (1984) 618.
- [4] B.A. Faddegon, C.K. Ross and D.W.O. Rogers, *Med. Phys.* 18 (1991) 727.
- [5] T.M. Jenkins, W.R. Nelson and A. Rindi (eds.), *Monte Carlo Transport of Electrons and Photons* (Plenum, New York and London, 1988).
- [6] W.R. Nelson, H. Hirayama and D.W.O. Rogers, SLAC-Report-265, Stanford Linear Accelerator Center (Dec. 1985).
- [7] M.J. Berger and S.M. Seltzer, *Phys. Rev. C* 2 (1970) 621.
- [8] J.A. Halbleib and T.A. Mehlhorn, Sandia Report SAND84-0573 (Nov. 1984).
- [9] R.L. Ford and W.R. Nelson, Stanford Linear Accelerator Center report SLAC-210 (1978).
- [10] S. Tanaka, R. Tanaka, T. Tabata, R. Ito, Y. Nakai and K. Ozawa, Japan Atomic Energy Research Institute report M83-019 (1983).
- [11] International Commission on Radiation Units and Measurements, ICRU report 37, October (1984).
- [12] S.M. Seltzer and M.J. Berger, *Nucl. Instr. Meth.* B12 (1985) 95.
- [13] K.C.D. Chan, M.A. Lone, S.E. Adams, P.Y. Wong, *Nucl. Instr. and Meth.* B10/11 (1985) 419.
- [14] E.J. Born, *Phys. Med. Biol.* 33 (1988) 55 (Abstract).
- [15] D.J.S. Findlay, *Nucl. Instr. and Meth.* A276 (1989) 598.
- [16] O. Sauer and M. Neumann, *Radioth. and Oncol.* 18 (1990) 39.
- [17] B.A. Faddegon, PhD thesis, Carleton University, Ottawa, Canada (1990). Also available as NRCC (Canada) report PIRS-0245 (1991).
- [18] B.A. Faddegon, C.K. Ross and D.W.O. Rogers, *Med. Phys.* 17 (1990) 773.
- [19] A.F. Bielajew and D.W.O. Rogers, *Nucl. Instr. and Meth.* B18 (1987) 165.
- [20] H.W. Koch and J.W. Motz, *Rev. Mod. Phys.* 31 (1959) 920.
- [21] A.F. Bielajew, R. Mohan and C.S. Chui, National Research Council of Canada internal report PIRS-0203 (1989).
- [22] S. Duane, A.F. Bielajew and D.W.O. Rogers, National Research Council of Canada report PIRS-0173 (1989).
- [23] D.W.O. Rogers, S. Duane, A.F. Bielajew and W.R. Nelson, National Research Council of Canada report PIRS-0177 (1989).
- [24] International Commission on Radiation Units and Measurements ICRU report 35, September (1984).
- [25] B.A. Faddegon, NRCC report PIRS 0313, December (1991).
- [26] J.A. Halbleib, R.P. Kensek, T.A. Mehlhorn, G.D. Valdez, S.M. Seltzer and M.J. Berger, Sandia report SAND91-1634, March (1992).